Geophysical Journal International

Geophys. J. Int. (2020) **222,** 735–742
Advance Access publication 2020 May 07
GJI Heat Flow and Volcanology

doi: 10.1093/gji/ggaa205

A model for the atmospheric shock wave produced by a strong volcanic explosion

Michele Dragoni and Dalila Santoro

Dipartimento di Fisica e Astronomia, Alma Mater Studiorum - Università di Bologna, Viale Carlo Berti Pichat 8, 40127 *Bologna, Italy. E-mail: michele.dragoni@unibo.it*

Accepted 2020 April 27. Received 2020 April 19; in original form 2020 February 24

SUMMARY

Atmospheric shock waves are a common phenomenon in explosive volcanic eruptions. We consider the motion of a spherical shock wave generated by a point source in the strong shock approximation. The shock front corresponds to discontinuities in the gas velocity, density, pressure and temperature, which are calculated as functions of the energy of the explosion. The problem is solved analytically for the distributions of velocity, density, pressure and temperature in the atmosphere as functions of the distance from the source. The motion of the shock wave being supersonic, the solution is valid for a few seconds after the explosion, corresponding to a distance of few kilometres. The acoustic effect of the shock wave, expressed by the peak sound pressure level, is calculated and may reach hundreds of decibels. The pressure waveform that could be recorded in the vicinity of the volcano is calculated and compared with typical waveforms in weak shock conditions. The change in the refractive index of air due to density inhomogeneity is calculated and the conditions under which a condensation cloud is formed behind the shock front are investigated.

Key words: Atmospheric effects (volcano); Explosive volcanism; Volcanic hazards and risks.

1 INTRODUCTION

Atmospheric shock waves are a common phenomenon in explosive volcanic eruptions, indicating that the erupting fluid at the vent is overpressurized with respect to the atmosphere (Ishihara 1985; Woods & Bower 1995). The air shock propagates ahead of the erupting fluid at a velocity exceeding the atmospheric sound speed and can have enough energy to rattle and even break windows at several kilometres from the crater (Baxter 2000; Morrissey & Mastin 2000). Shock waves are well documented for Plinian eruptions (Reed 1987) and have also been reported for Vulcanian eruptions (Nairn 1976; Yokoo & Ishihara 2007). Marchetti *et al.* (2013) presented evidence of infrasonic shock waves associated with Strombolian activity.

Field measurements of expanding shock waves can be directly recorded by pressure transducers or imaged under the proper illumination and atmospheric conditions (Morrissey & Chouet 1997). Air shocks are frequently recorded on microbarographs at distances greater than 50 km from the eruption vent. The explosions that destroyed the summit edifice of Krakatau in 1883 were among the greatest volcanic explosions ever documented, being audible up to 4600 km away and recorded on barographs around the world (Yokoyama 1981).

More recently, shock waves were recorded in several explosive eruptions. The 1958 eruption of Mount Asama (Japan) produced terrific detonations and air shocks that were heard at the foot of the volcano in an area 8–18 km away from the crater and caused damage to windows of houses as far out as 15 km (Baxter 2000).

During the 1975 Ngauruhoe eruption (New Zealand), the overpressure produced by the shock wave was recorded at a distance of 9 km from the vent and associated with a burst pressure of 5–6 MPa (Morrissey & Mastin 2000).

The activity of Sakurajima (Japan) is characterized by an eruption rate of up to 400 explosive events per year. The onset of the 1989 eruption was marked by a shock wave followed by the ejection of a pyroclastic cloud. From photographic analysis, the initial shock wave velocity was about 500 m s^{-1} (Morrissey & Mastin 2000).

The shock wave produced by the 1980 Mount St. Helens (USA) eruption was associated with a pressure release as large as 100 MPa. The wave amplitude was large enough to rattle windows up to 300 km away (Baxter 2000).

In years 1992–1993, the Galeras volcano (Columbia) produced six explosive eruptions. The first one destroyed the lava dome and generated shock waves that broke windows 9 km from the volcano (Vergniolle & Mangan 2000). At Galeras, historic eruptions are reported to have generated shock waves that knocked down people as far as 13 km from the vent (Baxter 2000).

Direct measurement of dynamic and thermodynamic quantities in a shock wave is strongly limited by the dramatic attenuation of such waves with distance, which corresponds to a rapid decrease in propagation velocity: thus, even relatively near-source sensors are

already too far away to detect a supersonic moving front. Therefore, most of available data concern weak shock waves.

However, optical effects that are produced by a shock wave may be often observed and can be used to investigate its properties. The shock wave can be momentarily visible above the volcano when it passes through clear air and condenses water vapour. The 1975 eruption of Ngauruhoe (New Zealand) was one of the first well-documented Vulcanian eruptions, with many large explosions from the summit crater (Nairn 1976). In a series of photographs of one explosion, taken by different observers, the passage of the shock front is manifested by the appearance of a short-lived, white condensation cloud immediately behind the shock front.

In strong explosions, the so-called flashing arcs may be also recorded with conventional cameras (Takayama & Saito 2004). They are explained with the sudden density change occurring across a shock wave and the consequent refraction of background light. Thanks to this optical effect, a shock wave was clearly observed in the 2014 eruption of the Tavurvur volcano, Papua, New Guinea (Bouvet de Maisonneuve *et al.* 2015).

Explanation of these phenomena requires a detailed modelling of the dynamic and thermodynamic quantities describing the shock wave in the first few seconds after its generation. Previous studies of volcanic shock waves did not consider this aspect analytically. A short review was given by Yokoo *et al.* (2006).

Myagkov (1998) employed a simplified model assuming that the entire mass of air encompassed by the shock wave is concentrated in a thin layer behind the shock front. The velocity and pressure were assumed to be constant in this layer and to be equal to the front values. The aim of the model was mainly the evaluation of the erupted mass.

Saito & Takayama (2005) developed a 3-D computer code simulating the propagation of blast waves generated by explosive volcanic eruptions. Application to an imaginary eruption of Mt. Fuji provided useful information regarding the wave interactions with local ground geometry.

Medici *et al.* (2014) used an open-ended shock tube to generate shock waves in the laboratory that are representative of explosive volcanic eruptions. They suggested that the strong shock wave approximation can be used for modelling moderate volcanic eruptions.

In this paper, a model for the atmospheric shock wave produced by a strong volcanic explosion is presented. The model is based on the theory of gas dynamics, considering the motion of an ideal, homogeneous and isotropic fluid. The problem was first considered by Latter (1955), Sedov (1959), Landau & Lifshitz (1987) and later by Kamm (2000). The dynamics of the shock wave is independent of the kind of explosion, whether mechanical, chemical or nuclear.

Under reasonable assumptions, the model has the merit of allowing a complete analytical solution. We derive expressions for the velocity of the shock front, as well as for velocity, density, pressure and temperature of the air behind the front. This region is virtually inaccessible during the shock wave propagation and the model allows to enlighten the relationships between the energy release and the characteristic of the shock wave, such as the magnitude of pressure and temperature discontinuities and their evolution in time. The acoustic effect of the shock in terms of the peak sound pressure level and the propagating pressure waveform are also calculated. Finally, optical effects such as the change in the refractive index of air and the generation of a condensation cloud behind the shock front are investigated.

2 THE MODEL

We develop a model for the shock wave under the assumption that the volcano is the source of a large amount of energy that is released in a very short time. In detail, the model assumptions are as follows: (1) the shock wave is strong; (2) the source is point-like, isotropic and impulsive; (3) the source is placed in an ideal, homogeneous and isotropic fluid; (4) the fluid is a perfect gas; (5) the interaction of the shock wave with the Earth's surface is negligible.

A shock wave is strong when the associated pressure discontinuity is large (Fox & McDonald 1985; Landau & Lifshitz 1987; Kundu 1990). More precisely, the condition is

$$p_2 \gg \frac{\gamma+1}{\gamma-1} p_1, \tag{1}$$

where p_1 and p_2 are the gas pressures immediately ahead and behind the shock front respectively and γ is the ratio between the specific heat capacities of the gas:

$$\gamma = \frac{c_p}{c_v}. \tag{2}$$

For air $\gamma = 1.4$, so p_2 must be at least six times greater than the atmospheric pressure p_1. In the case of strong explosions, condition (1) is satisfied in the proximity of the volcano, where pressure can reach values of tens of MPa (Fagents & Wilson 1993; Mason *et al.* 2004; Yokoo *et al.* 2006; Gudmundsson 2016). Since the shock wave attenuates rapidly with distance, assumption 1 implies that the model is valid at relatively short distances from the source and for a short time interval because the initial velocity is supersonic. From the following calculations it results that, even for large energy explosions, condition (1) is satisfied for a few seconds after the explosion.

As to assumption 2, it will be shown in Section 4 that the pressure waveform generated by the explosion is a sharp pulse with a duration of a fraction of second. The spectrum of a pulse with duration Δt is dominated by wavelengths $\lambda > u\Delta t$, where u is the propagation velocity. The validity of the point-like assumption at distance r_0 from the source can be estimated from the Fraunhofer condition (Aki & Richards 2002)

$$L^2 \ll \frac{\lambda r_0}{2}. \tag{3}$$

With $\Delta t = 10^{-1}$ s, $u = 10^3$ m s^{-1} and r_0 ranging from 1 to 5 km, it results $L \ll 200$ to 500 m, which can be considered acceptable for large explosions.

As to the assumption of source isotropy, real explosions may be irregular and characterized by directionality. Kim *et al.* (2012) studied the acoustic emissions in the infrasound band of Tungurahua volcano, Ecuador, and found that the source could be represented by a dipole, showing a good agreement with the opening direction of the vent. Multipole sources were considered by Iezzi *et al.* (2019) in modelling the acoustic emissions of Yasur volcano, Vanuatu.

Assumptions 3 and 5 are consistent with the strong shock assumption: considering the motion over a short distance and a short lapse of time allows the assumption of an ideal, homogeneous and isotropic fluid, implying that absorption is neglected, as well as variations of density, pressure and temperature with the elevation above sea level and the effects of reflection at the Earth's surface.

When a shock wave meets the surface of a solid body, the line of intersection is accompanied by reflection of the shock wave. For a strong shock wave, regular reflection takes place only if the intersection angle does not exceed about 40°: for higher values, the incident shock wave breaks up and a complicated pattern results, which is

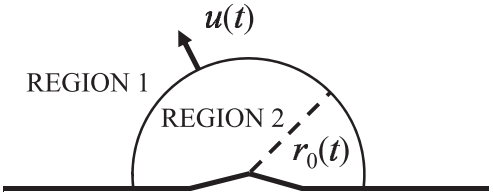

Figure 1. Sketch of the model. The shock wave is a spherical surface of radius r_0 expanding at velocity u.

called Mach reflection (Hornung 1986). In the flat ground approximation (Fig. 1), intersection occurs at about 90° and reflection is negligible. Consideration of topography may alter this conclusion: acoustic waveform inversion of infrasound data demonstrate that topographic effects can be relevant (Kim *et al.* 2015).

Assumption 4 is also commonly used in problems of gas dynamics: in the case of a shock wave, it is acceptable because the relatively high pressures produced behind the shock front are associated with high temperatures, so that air can be still approximated as a perfect gas.

As a consequence of assumptions 2 and 3, the shock wave is a spherical surface (Fig. 1). Accordingly, a system of spherical coordinates is introduced. It is supposed that the source is at the origin and releases an energy E at time $t = 0$. Let r be the distance from the origin and $r_0(t)$ be the position of the shock wave. The regions $r > r_0$ and $r < r_0$ are called region 1 and region 2, respectively.

The gas is described by its density ρ, pressure p, temperature T, entropy s per unit mass, specific heat capacities c_p and c_v. For a perfect gas

$$s = c_v \ln \frac{p}{\rho^\gamma}. \tag{4}$$

Let ρ_1, p_1 and T_1 be the initial values of density, pressure and temperature of the gas, respectively: they are the values in region 1, where they are uniform according to assumption 3. However, the three variables are discontinuous across the shock wave. We call ρ_2, p_2 and T_2 their values at $r = r_0 -$.

Let v be the velocity of the gas, v_1 its value in region 1 and v_2 its value at $r = r_0 -$. In the strong shock wave approximation, the values v_2, ρ_2, p_2 and T_2 are given by the Rankine–Hugoniot relationships

$$v_2 = \frac{2}{\gamma + 1} u \tag{5}$$

$$\rho_2 = \frac{\gamma + 1}{\gamma - 1} \rho_1 \tag{6}$$

$$p_2 = \frac{2}{\gamma + 1} \rho_1 u^2 \tag{7}$$

$$T_2 = \frac{(\gamma - 1) p_2}{(\gamma + 1) p_1} T_1, \tag{8}$$

where u is the velocity of the shock wave. Except for ρ_2, these values are functions of time which can be made explicit if one knows the shock velocity u, which is calculated in the next section.

Velocity v, density ρ and pressure p in region 2 can be obtained by solving three partial differential equations: the equation of motion, the equation of continuity and the equation of entropy (Landau & Lifshitz 1987). The unknown functions v, ρ and p depend only on the coordinate r, so that the three equations are

$$\frac{\partial v}{\partial t} + v \frac{\partial v}{\partial r} = -\frac{1}{\rho} \frac{\partial p}{\partial r} \tag{9}$$

$$\frac{\partial \rho}{\partial t} + \frac{2 \rho v}{r} + \frac{\partial}{\partial r}(\rho v) = 0 \tag{10}$$

$$\left(\frac{\partial}{\partial t} + v \frac{\partial}{\partial r} \right) \ln \frac{p}{\rho^\gamma} = 0. \tag{11}$$

From the knowledge of ρ and p, temperature T can be obtained from the equation of state

$$\frac{p}{\rho} = m R T, \tag{12}$$

where m is the number of moles per unit mass and R is the gas constant. The method of solution is given in the Appendix. The gas velocity v, density ρ, pressure p and temperature T in region 2 are obtained as functions of a non-dimensional variable

$$\xi = \frac{r}{r_0} \tag{13}$$

ranging from 0 to 1. The four variables, expressed as ratios to their values immediately behind the front, are

$$\frac{v}{v_2} = \frac{\gamma + 1}{2} V \xi \tag{14}$$

$$\frac{\rho}{\rho_2} = \frac{\gamma - 1}{\gamma + 1} G \tag{15}$$

$$\frac{p}{p_2} = \frac{\gamma + 1}{2\gamma} \frac{\rho}{\rho_1} Z \xi^2 \tag{16}$$

$$\frac{T}{T_2} = \frac{\rho_2}{p_2} \frac{p}{\rho}, \tag{17}$$

where V, G and Z are functions of ξ defined in the Appendix.

3 DISCUSSION

Density, pressure and temperature in region 1 have the unperturbed values ρ_1, p_1 and T_1, respectively. We take the values for air at sea level, which are $\rho_1 = 1.225$ kg m^{-3}, $p_1 = 101$ kPa and $T_1 = 288$ K. In a reference system fixed to the ground, the gas velocity v_1 is assumed to be zero.

A crucial parameter is the amount of kinetic energy E released by the explosion. In the 1980 Mount St. Helens explosion, wave amplitudes at 50–300 km distance were about what might be expected from a nuclear explosion of between 1 and 10 Mton yield (Reed 1987). A value of 7 Mton was estimated by Kieffer (1981), corresponding to $E \simeq 3 \times 10^{16}$ J. At the upper boundary of kinetic energy, observations of broken window panes 100 miles away from the 1883 Krakatau eruption can be used (Galanopoulos & Bacon 1970). On this basis, Kozlov *et al.* (1994) estimated an energy release of 370 Mton, corresponding to $E \simeq 1.5 \times 10^{18}$ J. Accordingly, for medium-size to large-size eruptions, an energy release E ranging between 10^{16} and 10^{18} J will be assumed. The total thermal energy release can be two or three orders of magnitude greater (Pyle 2000).

In Fig. 2, the velocity u of the shock wave and the distance r_0 travelled by the shock front are shown as functions of time, for different values of the energy E. The ratio u/c_1 is plotted in Fig. 2(a), where c_1 is the sound velocity in region 1:

$$c_1 = \sqrt{\frac{\gamma p_1}{\rho_1}}. \tag{18}$$

Supersonic velocities are maintained for a few seconds, according to the energy of the explosion. The corresponding distances travelled by the front, amounting to a few kilometres, are shown in Fig. 2(b).

We next consider the discontinuities of dynamic and thermodynamic variables across the shock wave. While the variables at $r =$

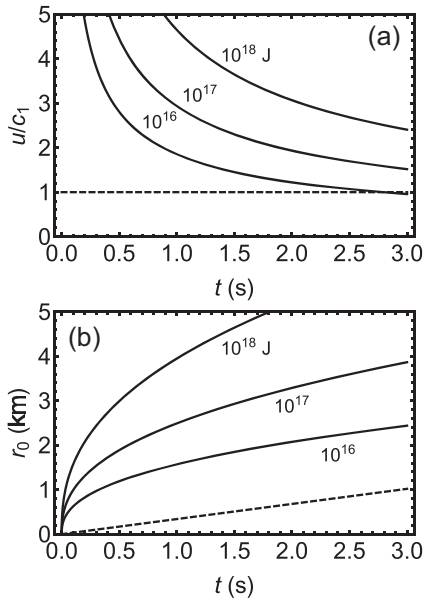

Figure 2. (a) Velocity u of the shock wave in units of the sound velocity c_1 and (b) distance r_0 travelled by the shock wave, as functions of time t. The curves refer to different values of the energy release E. The dashed lines are respectively the sound velocity and the distance travelled by sound.

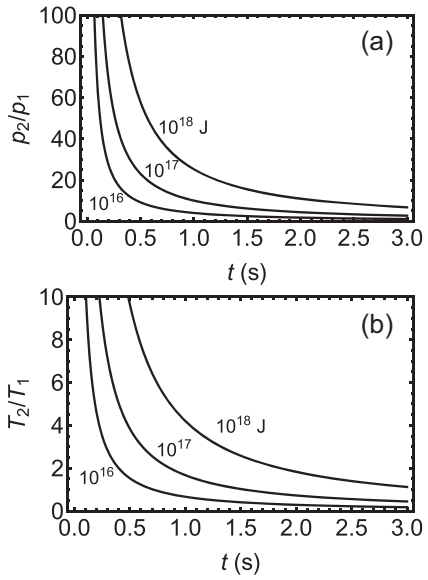

Figure 3. (a) Pressure p_2 and (b) temperature T_2 immediately behind the shock wave in units of their values p_1 and T_1 in region 1, as functions of time, for different values of energy E.

r_0+ are constant, their values at $r = r_0-$ are in general functions of time. An exception is density ρ_2, which is constant and equal to $6\rho_1$, as given by eq. (6). The pressure and temperature discontinuities are determined by the energy E and can be arbitrarily large.

From eqs (7), (A4), (A2) and (A1), pressure p_2 as a function of time is

$$p_2 = \frac{8}{25}\frac{\beta^2}{\gamma+1}\left(\frac{E^2\rho_1^3}{t^6}\right)^{1/5} \tag{19}$$

and temperature T_2 is obtained from eq. (19) according to eq. (8). In Fig. 3, the ratios p_2/p_1 and T_2/T_1 are shown as functions of time, for different values of E. Both ratios tend rapidly to 1 following

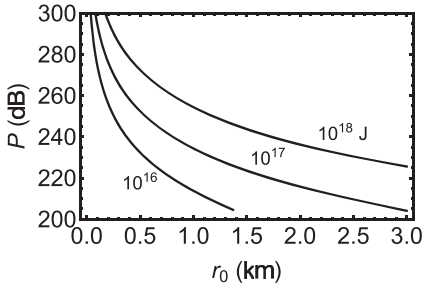

Figure 4. Peak sound pressure level P of the shock wave as a function of the wave radius r_0, for different values of energy E.

the attenuation of discontinuities. Velocity v_2 is proportional to the shock wave velocity u according to eq. (5).

The velocity and pressure values shown in Figs 2(a) and 3(a) are consistent with estimates of other authors. Calculations made by Wohletz *et al.* (1984) show that large caldera-forming eruptions with a magma chamber overpressure of 100 MPa form an air shock wave of 3 MPa (i.e. $p_2/p_1 \simeq 30$) with a velocity greater than 1 km s^{-1} (i.e. $u/c_1 > 3$).

The acoustic effect of the shock wave can be expressed by the peak sound pressure level, defined as (Pierce 1994)

$$P = 20 \log \frac{p_2 - p_1}{p_0}, \tag{20}$$

where p_0 is the threshold of audibility for pressure ($p_0 = 3 \times 10^{-5}$ Pa). From eq. (A2), when the wave front is at distance r from the source, the time elapsed from the explosion is

$$t_0 = \sqrt{\frac{\rho_1 r^5}{\beta^5 E}}. \tag{21}$$

From eq. (19) with $t = t_0$ and $r = r_0$, we obtain then

$$p_2 = \frac{8\beta^5 E}{25(\gamma+1)r_0^3}, \tag{22}$$

showing that p_2 decreases as the cube of the distance covered by the front. The peak sound pressure level P as a function of the shock wave radius r_0 is shown in Fig. 4 for different values of energy E. Sound pressure levels larger than 200 dB are predicted within some kilometres from the source.

For a comparison, the sound tolerance limit of the human ear is 120 dB, corresponding to an overpressure of about 30 Pa. According to Baxter (2000), shock waves with overpressures of 7 kPa, corresponding to $P = 170$ dB, may break windows and the threshold for rupture of the eardrum is 35 kPa ($P = 180$ dB). During the 1888–1890 eruptions at Vulcano (Italy), shock waves broke windows 7 km from the vent and during the 1992–1993 eruption of Galeras volcano (Colombia) a shock wave broke windows as far as 9 km (Morrissey & Mastin 2000), suggesting much higher pressure levels closer to the source.

The dynamic and thermodynamic variables in region 2 are shown in Fig. 5. Gas velocity v, density ρ, pressure p and temperature T are plotted as functions of ξ, in units of the respective values v_2, ρ_2, p_2 and T_2 at $\xi = 1-$, according to eqs (14)–(17). The plotted ratios are independent of energy E.

The gas velocity v has its maximum v_2 immediately behind the shock front and then decreases almost linearly, vanishing at $\xi = 0$ (Fig. 5a). A very rapid decrease in density ρ behind the front can be noted: almost all the gas is concentrated in a relatively thin layer.

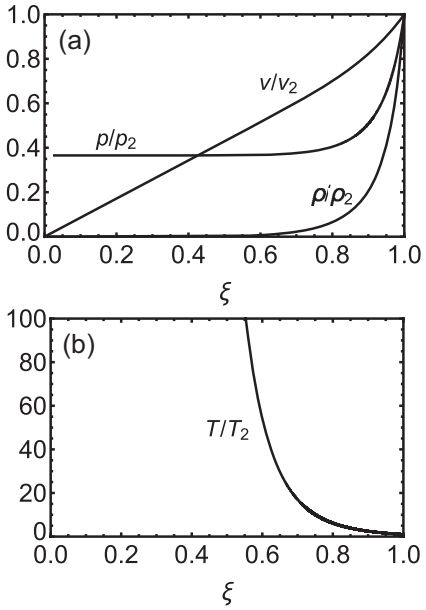

Figure 5. (a) Air velocity v, pressure p, density ρ and (b) temperature T behind the shock wave (region 2) as functions of the similarity variable ξ. The plotted ratios are independent of the energy release E.

This is related to the fact that the maximum density ρ_2 is six times the normal density ρ_1. Density vanishes at $\xi = 0$.

The ratio p/p_2 also decreases rapidly behind the front, but it approaches a constant value for $\xi \to 0$. From eq. (16), this constant is

$$k = 2^{-\frac{6}{5}} \left(\frac{2\gamma+1}{7-\gamma}\right)^{\alpha_6} \left(\frac{\gamma+1}{\gamma}\right)^{\alpha_7} \tag{23}$$

where α_6 and α_7 are given in the Appendix. The value of k depends only on γ and is equal to 0.365 for air (Fig. 5a).

On the contrary, temperature increases very rapidly as ξ decreases (Fig. 5b). Since pressure is a constant, while density vanishes at $\xi = 0$, temperature approaches infinity. However, it must be considered that the air is extremely rarefied in the proximity of the source during the shock wave propagation.

4 PRESSURE WAVEFORMS

The obvious way to measure shock wave intensity is by pressure sensors. However, shock fronts travelling at supersonic velocities have been only observed visually (Nairn 1976; Yokoo & Ishihara 2007), but never reported directly from pressure records, due to the rapid attenuation of shock waves with distance, which corresponds to a reduction in propagation velocity (Fig. 1a); thus, even the nearest sensors to the source are too far away to detect a supersonic moving front. In principle, thermal imagery could detect the pressure wave as soon as it exits the vent, but it has been used so far only for weak shock waves (Marchetti *et al.* 2013). Therefore observed and simulated (e.g. Morrissey & Chouet 1997) pressure waveforms do not correspond to the strong shock condition considered by the present model.

We define the pressure waveform as the function

$$p'(t) = p(t) - p_1. \tag{24}$$

An analytical expression for $p'(t)$ is not available in the general case. A theorem in gas dynamics (Landau & Lifshitz 1987) states that in a spherical shock wave the integral of p' over all time for a given r must be zero. Therefore, as a spherical wave passes through a given point, both compression ($p' > 0$) and rarefaction ($p' < 0$) will be observed. This behaviour is usually described by the empirical Friedlander function (Friedlander 1946):

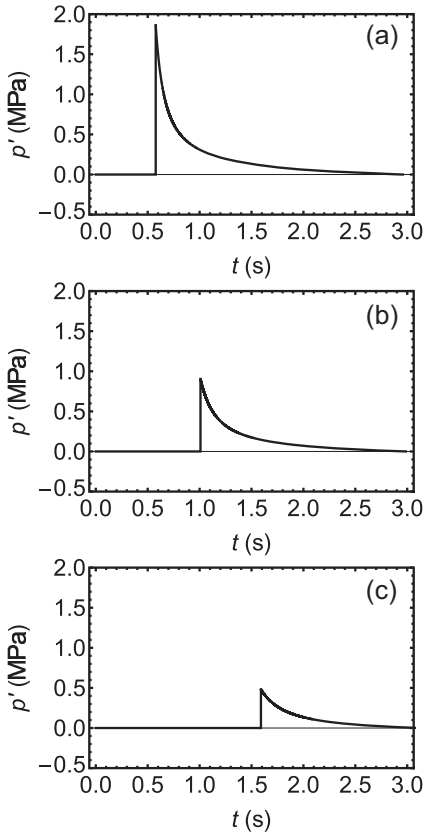

Figure 6. Pressure waveforms $p'(t)$ at different distances from the source: $r = 2$ km (a), 2.5 km (b), and 3 km (c). An energy $E = 10^{17}$ J is assumed.

$$p'(t) = p_0 \left(1 - \frac{t-t_0}{\tau}\right) \mathrm{e}^{-\frac{t-t_0}{\tau}}, \quad t \geq t_0, \tag{25}$$

where p_0 is the peak value recorded at $t = t_0$, when the wave reaches the observer, and τ is a characteristic time. However, for p_0 greater than about one atmosphere, the Friedlander function is no longer able to describe accurately the pressure time history (Dewey 2010).

The present model provides an analytical expression for the pressure waveform in strong shock conditions. At a generic distance r from the source, the waveform can be obtained from (16), (19), (15) and (13) as

$$p'(t) = \begin{cases} 0, & 0 < t < t_0 \\ \dfrac{4\rho_1 r^2}{25\gamma} \dfrac{GZ}{t^2} - p_1, & t > t_0 \end{cases}, \tag{26}$$

where G and Z are functions of time and t_0 is the time at which the wave reaches distance r, which is given by (21). Pressure waveforms at three different values of r are shown in Fig. 6, where the rapid decrease of the peak value $p_2 - p_1$ with distance is evident.

In strong shock conditions, the waveform is dominated by the compression phase: rarefaction takes place in a subsequent time, when condition (1) is no longer satisfied. A description of the shock wave in the short space and time interval, where it can be considered strong, is crucial for explaining the optical effects that are considered in the next section.

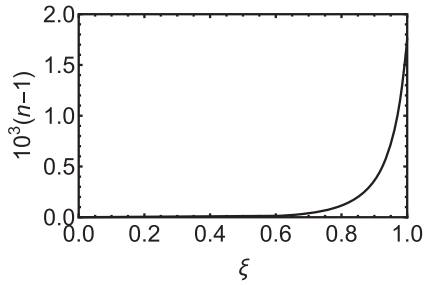

Figure 7. Refractive index n behind the shock wave (region 2) as a function of the similarity variable ξ.

5 OPTICAL EFFECTS

As mentioned in Section 1, in certain circumstances the shock wave can be observed directly, thanks to the change in the refractive index of air or the formation of a condensation cloud. The refractive index n is a function of density and increases with increasing density due to the corresponding decrease in the speed of light. The change is small and n can be expressed to a first approximation as a linear function of ρ (e.g. Edlén 1966):

$$n(\rho) = n_1 + \frac{\mathrm{d}n}{\mathrm{d}\rho}(\rho - \rho_1), \tag{27}$$

where

$$n_1 = n(\rho_1), \tag{28}$$

and

$$\frac{\mathrm{d}n}{\mathrm{d}\rho} = \frac{n_1 - 1}{\rho_1}. \tag{29}$$

Then, thanks to eq. (6),

$$n = n_1 + (n_1 - 1)\left(\frac{\gamma + 1}{\gamma - 1}\frac{\rho}{\rho_2} - 1\right) \tag{30}$$

where the ratio ρ/ρ_2 is given by eq. (15). The function $n(\xi) - 1$ is plotted in Fig. 7, showing that n is sensibly greater than 1 only in a thin shell behind the shock wave (approximately $0.9 < \xi < 1$). At $\xi = 1-$, the index has the value

$$n_2 = n_1 + 2\frac{n_1 - 1}{\gamma - 1} \tag{31}$$

that is about 0.15 per cent greater than n_1 and is equal to 1 at $\xi = 0$. The refractive index does not depend on the energy release E because the ratio ρ/ρ_2 is independent of E.

In order that condensation may occur, pressure p must exceed the vapour pressure p_v of water, which is an increasing function of temperature. Therefore, condensation is favoured by an increase in pressure and by a decrease in temperature. The passage of the shock wave produces a sudden increase both in pressure and temperature. Behind the front, pressure decreases while temperature increases, as shown in Fig. 5.

To ascertain whether vapour condensation may occur, pressure $p(\xi)$ must be compared with vapour pressure $p_v(\xi)$ in region 2 at different times during the motion of the shock wave. The dependence of p_v on T can be expressed by the approximate Magnus formula (Alduchov & Eskridge 1996):

$$p_v(T) = p_0 \mathrm{e}^{\frac{a(T-T_0)}{T-T_0+T^*}}, \tag{32}$$

where $p_0 = 610.94$ Pa, $a = 17.625$, $T_0 = 273.15$ K and $T^* = 243.04$ K.

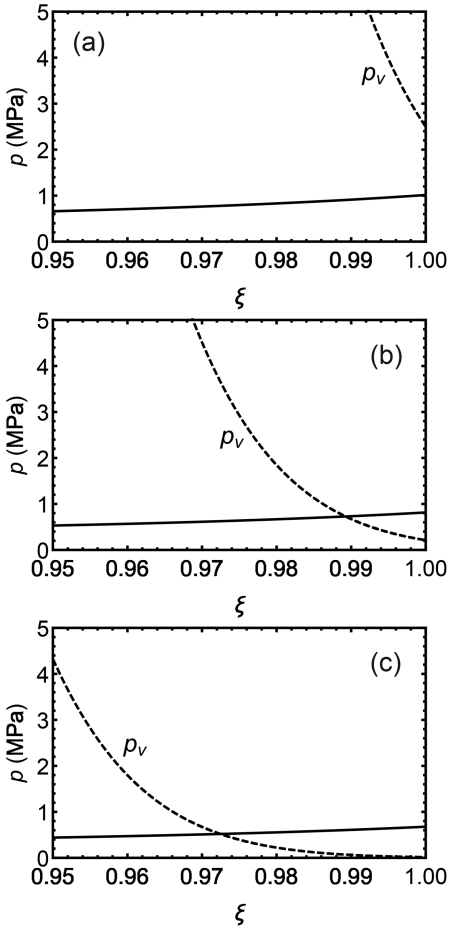

Figure 8. Air pressure p (solid curves) and vapour pressure p_v (dashed curves) behind the shock wave (region 2) as functions of the similarity variable ξ, at different times after the explosion: 1 s (a), 1.2 s (b), and 1.4 s (c). An energy $E = 10^{17}$ J is assumed.

From eq. (17), with T_2 depending on time according to eq. (8), we obtain $T(\xi)$. From eq. (32) we obtain then $p_v(\xi)$. As to pressure, we use solution (16) for $p(\xi)$, with p_2 depending on time according to eq. (7).

Graphs of the functions $p(\xi)$ and $p_v(\xi)$ for three values of time are shown in Fig. 8, in the case of an energy $E = 10^{17}$ J. Condensation starts at $\xi = 1-$, where pressure has the highest value and temperature has the lowest one. Initially, temperature T_2 can be very high, exceeding the critical temperature of water. As time increases, both T_2 and p_2 decrease, as shown in Fig. 3.

At $t = 1$ s, the values of temperature, vapour pressure and pressure at $\xi = 1-$ are $T_2 = 490$ K, $p_v = 2.5$ MPa and $p_2 = 1$ MPa, that is still smaller than p_v (Fig. 8a). But at $t = 1.2$ s the values are $T_2 = 394$ K, $p_v = 0.2$ MPa and $p_2 = 0.8$ MPa, that is greater than p_v. At this temperature, pressure is sufficiently high to produce condensation and the thickness of the condensation layer is about 1 per cent of the radius r_0 of the shock wave (Fig. 8b). At $t = 1.4$ s, the thickness is about 3 per cent (Fig. 8c). The lifetime of the layer is very short because the decrease of p_2 is very fast.

A comparison can be made with the largest 1975 explosion of Ngauruhoe (New Zealand), when a nearly spherical, hollow condensation cloud was observed about 1 s after the explosion (Nairn 1976). At that time, the shock wave velocity was estimated to be at least 600 m s^{-1}, or $u/c_1 \simeq 2$. According to Fig. 2, this velocity corresponds to an energy $E \simeq 10^{16}$ J and the distance r_0 covered by

the shock front at that time is approximately 1.5 km. One second later, the cloud had disappeared. This is consistent with eq. (19) and Fig. 3(a), showing that at $t = 2$ s pressure p_2 had decreased to less than 0.2 MPa.

This phenomenon can be also observed in lower energy events. In a Strombolian explosion of the Yasur volcano (Vanuatu), Marchetti *et al.* (2013) observed a condensation cloud with a thickness increasing in time, similarly to what is predicted by the present model. The cloud was ascribed to the compressive wave front, propagating at a velocity close to 400 m s^{-1} and causing instantaneous vapour condensation.

6 CONCLUSIONS

A model for the shock wave generated by an explosive volcanic eruption has been presented. Assuming that a large amount of energy is released by the eruption in a very short time, the strong shock wave approximation has been considered. The source has been assumed to be point-like and placed in a homogeneous and isotropic ideal fluid, considered as a perfect gas.

The model allows a theoretical study of a phenomenon that is frequently observed, but is hardly measured due to its unpredictability and short duration, as well as to the inaccessibility of the region behind the shock front. A merit of the model is that analytical solutions can be obtained for the dynamic and thermodynamic variables, allowing a detailed study of the relationships between them.

For the considered energy range, the shock wave velocity is supersonic for a few seconds after the explosion, during which the shock front covers a distance of a few kilometres. In the region behind the front, the air velocity, density and pressure are monotonically increasing functions of the distance from the source, reaching their maximum values immediately behind the front. Temperature is instead a decreasing function of distance. The amplitudes of discontinuities in gas velocity, pressure and temperature are functions of the energy release. The propagation of the shock wave is accompanied by a rapid decrease in the amplitude of such discontinuities.

The acoustic effect of the shock wave, expressed by the peak sound pressure level, has been calculated as a function of the distance travelled by the wave and yields very high values in the considered time interval. The pressure waveforms that could be recorded by pressure sensors in the vicinity of the volcano have been calculated and compared with typical waveforms in weak shock conditions.

Owing to the density inhomogeneity, the refractive index of the air is inhomogeneous in the region behind the shock wave. A thin shell with a higher value of the index is generated immediately behind the shock front. The model also predicts the formation of a thin condensation layer immediately behind the shock front, in agreement with observations.

We remark that the strong shock wave approximation is valid during the first few seconds of the shock wave propagation, as long as the pressure discontinuity is large. Later, the discontinuities in dynamic and thermodynamic variables gradually vanish and the wave becomes a weak shock, which must be treated differently.

ACKNOWLEDGEMENTS

The authors are grateful to Jean Virieux, Carl Tape, Emanuele Marchetti and two anonymous reviewers for constructive comments and helpful suggestions on the first version of the paper.

REFERENCES

Aki, K. & Richards, P.G., 2002. *Quantitative Seismology,* 2nd edn, University Science Books.

Alduchov, O.A. & Eskridge, R.E., 1996. Improved Magnus form approximation of saturation vapor pressure, *J. Appl. Meteorol.,* **35**(4), 601–609.

Baxter, P.J., 2000. Impacts of eruptions on human health, in *Encyclopedia of Volcanoes,* pp. 1035–1043, ed. Sigurdsson, H., Academic Press.

Bouvet de Maisonneuve, C., Costa, F., Patia, H. & Huber, C., 2015. Mafic magma replenishment, unrest and eruption in a caldera setting: insights from the 2006 eruption of Rabaul (Papua New Guinea), *Geol. Soc. Lond. Spec. Publ.,* **422**(1), 17–39.

Dewey, J.M., 2010. The shape of the blast wave: studies of the Friedlander equation, in *Proceedings of the 21st International Symposium on Military Aspects of Blast and Shock,* pp. 1–9, Israel.

Edlén, B., 1966. The refractive index of air, *Metrologia,* **2**(2), 71–80.

Fagents, S.A. & Wilson, L., 1993. Explosive volcanic eruptions. VII. The ranges of pyroclasts ejected in transient volcanic explosions, *Geophys. J. Int.,* **113,** 359–370.

Fox, R.W. & McDonald, A.T., 1985. *Introduction to Fluid Mechanics,* 3rd edn, John Wiley & Sons.

Friedlander, F.G., 1946. The diffraction of sound pulses. I. Diffraction by a semi-infinite plate, *Proc. R. Soc. A,* **186,** 322–344.

Galanopoulos, A.G. & Bacon, E., 1970. *Atlantis, the Truth behind the Legend,* Nelson.

Gudmundsson, A., 2016. The mechanics of large volcanic eruptions, *Earth-Sci. Rev.,* **163,** 72–93.

Hornung, H., 1986. Regular and Mach reflection of shock waves, *Annu. Rev. Fluid Mech.,* **18,** 33–58.

Iezzi, A.M., Fee, D., Kim, K., Jolly, A.D. & Matoza, R.S., 2019. Three-dimensional acoustic multipole waveform inversion at Yasur volcano, Vanuatu, *J. geophys. Res.,* **124,** 8679–8703.

Ishihara, K., 1985. Dynamical analysis of volcanic explosion, *J. Geodyn.,* **3,** 327–349.

Kamm, J.R., 2000. Evaluation of the Sedov-von Neumann-Taylor blast wave solution, Los Alamos Scientific Laboratory Report LA-UR-00-6055.

Kieffer, S.W., 1981. Fluid dynamics of the May 18 blast at Mount St. Helens, U.S. Geol. Surv. Prof. Pap. 1250, pp. 379–400.

Kim, K., Lees, J.M. & Ruiz, M., 2012. Acoustic multipole source model for volcanic explosions and inversion for source parameters, *Geophys. J. Int.,* **191,** 1192–1204.

Kim, K., Fee, D., Yokoo, A. & Lees, J.M., 2015. Acoustic source inversion to estimate volume flux from volcanic explosions, *Geophys. Res. Lett.,* **42,** 5243–5249.

Kozlov, I.M., Romanov, G.S. & Suvorov, A.E., 1994. Numerical simulation of gasdynamics processes in the case of catastrophic volcanic eruption, *J. Eng. Phys. Thermophys.,* **66,** 229–232.

Kundu, P.K., 1990. *Fluid Mechanics,* Academic Press.

Landau, L.D. & Lifshitz, E.M., 1987. *Fluid Mechanics,* 2nd edn, Pergamon Press.

Latter, R., 1955. Similarity solution for a spherical shock wave, *J. Appl. Phys.,* **26,** 954–960.

Marchetti, E., Ripepe, M., Delle Donne, D., Genco, R., Finizola, A. & Garaebiti, E., 2013. Blast waves from violent explosive activity at Yasur Volcano, Vanuatu, *Geophys. Res. Lett.,* **40,** 5838–5843, .

Mason, B.G., Pyle, D.M. & Oppenheimer, C., 2004. The size and frequency of the largest explosive eruptions on Earth, *Bull. Volcanol.,* **66,** 735–748.

Medici, E.F., Allen, J.S. & Waite, G.P., 2014. Modeling shock waves generated by explosive volcanic eruptions, *Geophys. Res. Lett.,* **41,** 414–421.

Morrissey, M.M. & Chouet, B.A., 1997. Burst conditions of explosive volcanic eruptions recorded on microbarographs, *Science,* **275,** 1290–1293.

Morrissey, M.M. & Mastin, L.G., 2000. Vulcanian eruptions, in *Encyclopedia of Volcanoes,* pp. 463–475, ed. Sigurdsson, H., Academic Press.

Myagkov, N., 1998. Model of a strong volcanic blast and a method of estimating the mass ejected, *Geophys. J. Int.,* **133,** 209–211.

Nairn, I.A., 1976. Atmospheric shock waves and condensation clouds from Ngauruhoe explosive eruption, *Nature,* **259,** 190–191.

Pierce, A.D., 1994. *Acoustics: an Introduction to Its Physical Principles and Applications,* Acoustical Society of America.

Pyle, D.M., 2000. Sizes of volcanic eruptions, in *Encyclopedia of Volcanoes,* pp. 263–269, ed. Sigurdsson, H., Academic Press.
Reed, J.W., 1987. Air pressure waves from Mount St. Helens eruptions, *J. geophys. Res.,* **92**(D10), 11 979–11 992.
Saito, T. & Takayama, K., 2005. Applying shock-wave research to volcanology, *Comput. Sci. Eng.,* **7,** 30–35.
Sedov, L.I., 1959. *Similarity and Dimensional Methods in Mechanics,* Academic Press.
Takayama, K. & Saito, T., 2004. Shock wave/geophysical and medical applications, *Annu. Rev. Fluid Mech.,* **36,** 347–79.
Vergniolle, S. & Mangan, M., 2000. Hawaiian and Strombolian eruptions, in *Encyclopedia of Volcanoes,* pp. 447–461, ed. Sigurdsson, H., Academic Press.
Wohletz, K.H., McGetchin, T.R., Sandford, M.T. & Jones, E.M., 1984. Hydrodynamic aspects of caldera-forming eruptions: numerical models, *J. geophys. Res.,* **89**(B10), 8269–8285.
Woods, A.W. & Bower, S.M., 1995. The decompression of volcanic jets in a crater during explosive volcanic eruptions, *Earth planet. Sci. Lett.,* **131,** 189–205.
Yokoo, A., Ichihara, M., Goto, A. & Taniguchi, H., 2006. Atmospheric pressure waves in the field of volcanology, *Shock Waves,* **15**(5), 295–300.
Yokoo, A. & Ishihara, K., 2007. Analysis of pressure waves observed in Sakurajima eruption movies, *Earth Planets Space,* **59,** 177–181.
Yokoyama, I., 1981. A geophysical interpretation of the 1883 Krakatau eruption, *J. Volc. Geotherm. Res.,* **9,** 359–378.

APPENDIX: METHOD OF SOLUTION

Eqs (9)–(11) can be solved by the similarity approach (e.g. Sedov 1959), based on the fact that the only length scale in the problem is

$$L = \left(\frac{Et^2}{\rho_1}\right)^{1/5}. \tag{A1}$$

The position $r_0(t)$ of the shock wave must also scale with L and we can write

$$r_0 = \beta L, \tag{A2}$$

where β is a constant that can be calculated numerically from the conservation of energy. Its value for air is 1.033 (Landau & Lifshits 1987).

The shock wave velocity u can be obtained by differentiating (A2) with respect to time:

$$u(t) = \frac{2}{5}\beta\left(\frac{E}{\rho_1 t^3}\right)^{1/5} \tag{A3}$$

or

$$u(t) = \frac{2}{5}\frac{r_0(t)}{t}. \tag{A4}$$

Thanks to (A3), we can obtain v_2, p_2 and T_2 as functions of time from eqs (5), (7) and (8), respectively.

Following Landau & Lifshitz (1987), eqs (9)–(11) can be expressed in non-dimensional form. In the place of pressure, we use the square of the sound velocity

$$c^2 = \frac{\gamma p}{\rho} \tag{A5}$$

and introduce the non-dimensional variables V, G and Z, defined as follows:

$$v = \frac{2r}{5t}V \tag{A6}$$

$$\rho = \rho_1 G \tag{A7}$$

$$c^2 = \frac{4r^2}{25t^2}Z. \tag{A8}$$

As the variable ξ varies from 0 to 1, they range in the intervals

$$\frac{1}{\gamma} \le V \le \frac{2}{\gamma+1} \tag{A9}$$

$$0 \le G \le \frac{\gamma+1}{\gamma-1} \tag{A10}$$

$$\infty > Z \ge \frac{2\gamma(\gamma-1)}{(\gamma+1)^2}. \tag{A11}$$

Introduction of eqs (A6)–(A8) into eqs (9)–(11) yields a system of ordinary differential equations for V, G and Z as functions of ξ:

$$\gamma(1-V)V\left(1+\frac{\mathrm{d}\ln V}{\mathrm{d}\ln\xi}\right) = Z\left(2+\frac{\mathrm{d}\ln Z}{\mathrm{d}\ln\xi}+\frac{\mathrm{d}\ln G}{\mathrm{d}\ln\xi}\right) \tag{A12}$$

$$\frac{\mathrm{d}V}{\mathrm{d}\ln\xi} - (1-V)\frac{\mathrm{d}\ln G}{\mathrm{d}\ln\xi} = -3V \tag{A13}$$

$$\frac{\mathrm{d}\ln Z}{\mathrm{d}\ln\xi} - (\gamma-1)\frac{\mathrm{d}\ln G}{\mathrm{d}\ln\xi} = -\frac{5-2V}{1-V}. \tag{A14}$$

The solution of the system yields ξ, G and Z as functions of V:

$$\xi(V) = \left(\frac{\gamma+1}{2}V\right)^{-2/5} A^{\alpha_1} B^{\alpha_2} \tag{A15}$$

$$G(V) = \frac{\gamma+1}{\gamma-1}A^{\alpha_3} B^{\alpha_4} C^{\alpha_5} \tag{A16}$$

$$Z(V) = \frac{\gamma(\gamma-1)(1-V)V^2}{2(\gamma V-1)}, \tag{A17}$$

where A, B and C are linear functions of V, while α_1, α_2, α_3, α_4 and α_5 are constants, which are defined as

$$A(V) = \frac{(\gamma+1)(\gamma V-1)}{\gamma-1} \tag{A18}$$

$$B(V) = \frac{(\gamma+1)[5-(3\gamma-1)V]}{7-\gamma} \tag{A19}$$

$$C(V) = \frac{(\gamma+1)(1-V)}{\gamma-1} \tag{A20}$$

$$\alpha_1 = \frac{\gamma-1}{2\gamma+1}, \quad \alpha_2 = -\frac{13\gamma^2-7\gamma+12}{5(3\gamma-1)(2\gamma+1)},$$
$$\alpha_3 = \frac{3}{2\gamma+1} \tag{A21}$$

$$\alpha_4 = \frac{13\gamma^2-7\gamma+12}{(2-\gamma)(3\gamma-1)(2\gamma+1)}, \quad \alpha_5 = -\frac{2}{2-\gamma} \tag{A22}$$

$$\alpha_6 = \frac{13\gamma^2-7\gamma+12}{5(2-\gamma)(3\gamma-1)}, \quad \alpha_7 = \frac{4\gamma}{3\gamma-1}. \tag{A23}$$

The gas velocity v, density ρ, pressure p and temperature T in region 2 are then obtained as functions of V from eqs (A6), (A7), (A5) and (12), respectively. Their expressions are given by eqs (14)–(17). Each value of V in the interval (A9) corresponds to a value of ξ according to eq. (A15). Then the four variables can be plotted as functions of ξ.